Journal of Visualization, Vol. 12, No. 4 (2009) 307-321

Regular Paper

Interacting Wakes of Two Normal Flat Plates

An investigation based on phase averaging of LDA signals

Auteri, F.*, Belan, M.*, Cassinelli, C.* and Gibertini, G.*

* Politecnico di Milano, Dipartimento di Ingegneria Aerospaziale
Via La Masa 34, 20156 Milano, Italy.
E-mail: Franco.Auteri@polimi.it, Marco.Belan@polimi.it, Giuseppe.Gibertini@polimi.it

Received 19 December 2008
Revised 26 March 2009

Abstract : The flow around two bluff bodies in tandem is an interesting phenomenon whose nature strongly depends on the distance between the bodies. In this work oil smoke visualizations of the flow around two normal flat plates in tandem configuration are compared with phase averaged Laser Doppler Anemometry measurements of the flow field for a full period. Phase averaging is exploited to resolve the mean time evolution of the flow and the signal from a single constant temperature hot wire probe is employed as phasing reference. The flow-field information obtained from visualizations agrees well with quantitative indications provided by measures, and the comparison allows to precisely understand what information can be extracted from simple visualizations. As a result, new insight in flow mechanism is obtained from the analysis of the flow data showing that, for the analyzed plate distance, the gap between the two plates behaves substantially as a cavity while the vortex formation process takes place in the wake region behind the aft plate.

Keywords : Flat Plate, Bluff bodies, Wake Interference, Laser Doppler Anemometry, Phase averaging.

1. Introduction

The interaction between the wakes of two bluff bodies is of interest for many engineering fields and in particular for evaluating wind loads on large civil structures. Of course, every final application is characterized by a specific geometry and, as a consequence, by a specific wake behavior. Nevertheless, a deep understanding of the flow behavior around some reference geometries can be quite useful to usefully approach many engineering problems. In other words, a detailed description of the flow around a few simple reference geometries allows to understand the different flow phenomena that can be faced in real world applications. One geometry of particular interest is that of two slender bodies in tandem configuration. In particular, this work is concerned with two normal flat plates.

A distinctive feature of the flow around two bluff bodies in tandem configuration is that the nature of the flow changes with the their distance. As is the case for other bluff bodies in tandem configuration, such as circular cylinders (Zdravkovich, 1977; Igarashi, 1981, 1984; Xu and Zhou, 2004), rectangles (Takeuchi, 1988) or squares (Liu et al., 1999), also in this case the Strouhal number strongly depends on the distance between the two bodies. In figure 1 the variation of the Strouhal number (St= $f\,c\,/\,V_\infty$) with the distance between two normal flat plates is reported; here f is the frequency associated to the main peak in the power spectrum of the HWA signal and V_∞ is the free

stream velocity; Strouhal numbers will be presented in terms of their ratio to the single plate Strouhal number, St_{ref}, for convenience. As for other bluff bodies (Liu and Chen, 2002; Jester and Kallinderis, 2003), also in this case hysteresis or bistability is observed for intermediate distances. While for more complex geometries several flow regimes may exist (Havel et al., 2001), for flat plates two distinct flow regimes have been observed for short and long distances between the plates, similarly to what found by Xu et al. (2004) for circular cylinders. For a distance between the plates below the value of the plate chord, the Strouhal number is quite close to the single plate one, St/St_{ref} =1.03. This is a "one body mode" (Havel et al., 2001), or "mode I" as defined by Liu and Chen (2002) and hereafter. When the distance is increased over a threshold that slightly depends on Reynolds number, the Strouhal number grows through a discontinuity, to rapidly decrease as the distance is further increased, reaching a minimum for $3 \leq D/c \leq 4$. Afterwards, the Strouhal number starts to increase again and it seems to asymptotically approach the single plate one for distances greater than 8 *c*. Above the threshold distance the flow configuration changes, in fact the shear layer detaching from the fore plate roll-up between the plates. For this flow configuration, that will be denoted as "mode II" (Liu and Chen, 2002), a strong periodicity can be deduced from the sharp peak in the power spectral density of the HWA signal, while mode I presents a less sharp peak suggesting a less marked periodicity. In the region of non-dimensional distance values near one, the two flow configurations are both stable and the flow switches from one to another randomly. The amplitude and position of this bistability region slightly depends on the Reynolds number.

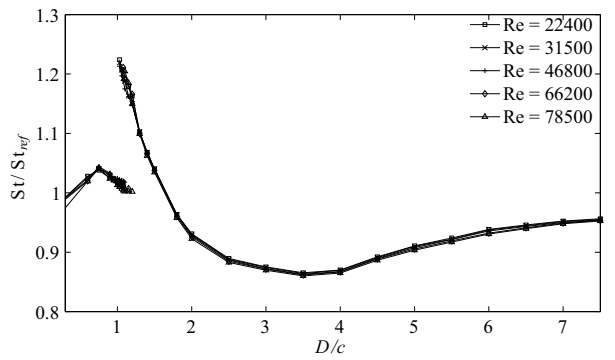

Fig. 1. Strouhal number, as a fraction of the single plate Strouhal number St_{ref}, versus distance between the plates.

The turbulent flow past bluff bodies is generally characterized by strong unsteadiness presenting essentially periodic large scale coherent structures together with more chaotic, turbulent, small scale structures. Thus the time averaged flow is rather meaningless as it is too different from the real instantaneous flow. Much more information can be obtained by analyzing the fundamental periodic (or quasi-periodic) mode. To extract the fundamental periodic motion from experimental data, ensemble averages of entire flow periods must be calculated. Ensemble average can be useful with both point-wise measurement techniques, such as Laser Doppler Anemometry (LDA), and global measurement techniques such as Particle Image Velocimetry, see for instance (Kim et al., 2002), that require averaging to obtain reliable statistics. In the averaging process, the relative phase of each piece of data with respect to the dynamics of the whole phenomenon must be preserved. This approach is called phase averaging.

Phase averaging techniques are usually employed to investigate physical problems where periodicity is provided by an external forcing that can be taken as a reference for synchronization. This is the case, for instance, of turbo machinery (Göttlich et al., 2004) or helicopter rotors (Seelhorst et al., 1994). On the contrary, when it comes to vortex shedding, periodicity arises from an intrinsic instability of the flow and no external reference is available. In this case, the reference signal has necessarily to be a measurable property of the flow itself, be it punctual, e.g. the modulus of the velocity vector in a specified point, or integral, e.g. the lift force acting on a body. In fact, to properly carry out the phase averaging, the LDA signals measured in different points must be referred to a common reference closely linked to the physics of the problem. In this way, minimum variations of

the main harmonic period, which is not strictly fixed, can be followed. For instance, a Hot Wire Anemometer (HWA) signal roughly measuring the velocity modulus, acquired simultaneously with the LDA measures, allows reconstructing the mean periodic flow by the phase averaging technique. For instance Cantwell and Coles (1983) investigated the near wake of a circular cylinder at Re=140000 by means of a flying X wire technique. In this case the phasing signal comes from a pressure measurement on the cylinder surface 65° away from the forward stagnation point. A similar technique has been employed by Perry and Steiner (1987) to investigate the wake of a flat plate both normal and inclined with respect to the free stream velocity for a Reynolds number near 20000. In this case, point measures are phased by the signal from a single HWA. The measures allow the authors to thoroughly describe the wake behavior within a few chord lengths aft the body. Kiya and Matsumura apply the phase averaging technique to a flat plate normal to the free stream velocity for a Reynolds number Re=23000. The phasing signal is the vertical component of the velocity, measured by an X-wire probe on the symmetry axis in the plate wake, while measurement points are obtained by traversing a LDA on a single line normal to the free stream, positioned 8 chord lengths aft the plate. The wake structures are then recovered by applying Taylor's hypothesis. LDA has been employed also by Lyn et al. (1995) who investigate the turbulent near wake of a square cylinder. In this case phasing is obtained exploiting the signal from a pressure tap positioned on the midpoint of a cylinder sidewall.

In the present work, these concepts are applied to the LDA investigation of the flow around two flat plates in tandem configuration normal to the free stream velocity for a plate distance D=0.9c, see figure 2 and 3, where c is the plate chord. The main goal of the present work is to thoroughly describe the mode I flow behavior through a full mean period by velocity, vorticity and RMS fields and by comparison with low exposure time high quality smoke visualizations. Phase averaged measurements for D=1.2c are also provided to compare mode I and mode II.

The paper is organized as follows. In section 2 the experimental set-up and test procedures are illustrated. In section 3 the phase averaging technique employed is recalled. In section 4 visualizations are reported. In section 5 mean and phase averaged velocity, vorticity and RMS fields are reported. In section 6 measurements for mode I flow configuration are compared with visualizations and measurements of mode II. In section 7 some concluding remarks are drawn.

2. The Experimental setup and test procedures

The two flat plates at 90° incidence in tandem arrangement are placed in an open loop wind tunnel with a test section of width equal to 500 mm and height equal to 700 mm. The turbulence level of the wind tunnel is less than 0.2%. The plates have a span of 500 mm and a chord of 70 mm, which give an aspect ratio of 7.1 and a solid blockage of 10%. The upstream plate is fixed in the test section while the other is mounted on sliding guides allowing the reciprocal distance to be varied.

Preliminary tests have been carried out with the upstream plate only, placing the probe of a constant temperature hot wire anemometer near the top of the upstream flat plate (see fig. 2).

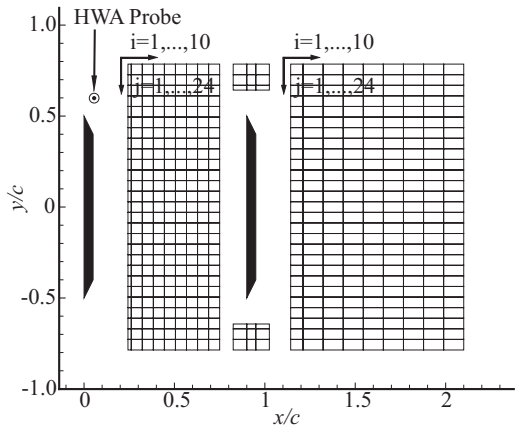

Fig. 2. LDA measurement grid and HWA probe position.

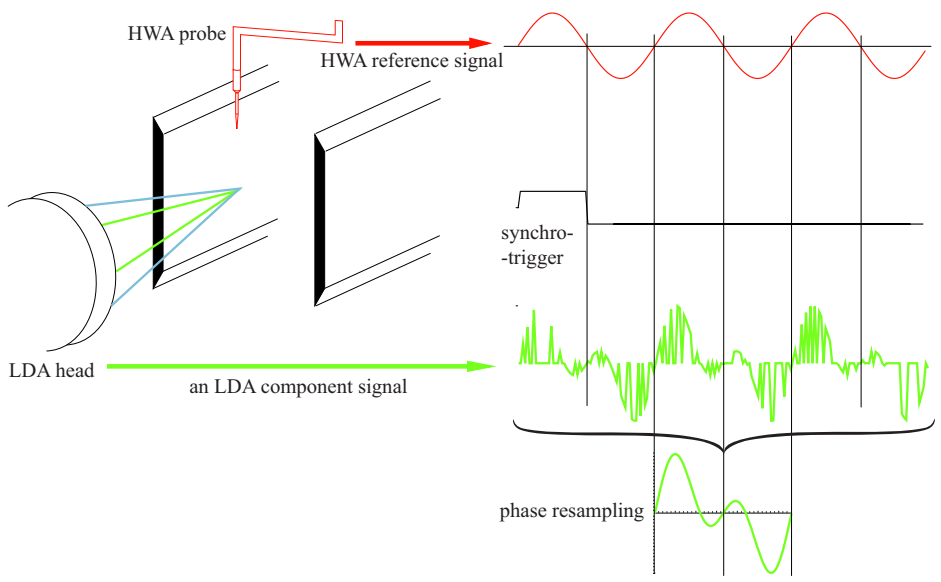

Fig. 3. Physical approach to phase averaging techniques on LDA signals.

A Strouhal number St_{ref}=0.158 was found on the base of the HWA signal power spectrum, independent of Reynolds number Re = $V_\infty\, c\,/\nu$ within the examined range $8.7\ 10^3 < Re < 7.5\ 10^4$. The value corrected for solid blockage by the formula proposed by Ota et al. (1994) is 0.138, which agrees well with the blockage free value of 0.136 reported by Chen and Fang (1996). In the following it will be used as a reference to bypass blockage issues.

Oil smoke visualizations have been obtained by a high speed Phantom v. 5.1 camera, featuring a 1024x1024 pixel, 8 bit CMOS color sensor. Oil smoke was produced by heating a diethylene-glycol water solution and injected upstream of the settling chamber screens. Lighting was provided by an argon laser light sheet that enabled the exposure time to be taken as low as 500 μs, so that small scale structures could be observed. To enable detail resolution, the Reynolds number of smoke visualizations was lower than that of the measurements, namely 16850. The frame rate was 600 fps, and thus enabled to take 72 frames per period, allowing an accurate comparison between visualizations and phase averages.

Point-wise velocity measurements in the symmetry plane normal to the plate axes were performed using a double component DANTEC Dynamics Laser Doppler Anemometer, making use of an Argon laser light source and configured in backward scatter mode. Optics were mounted on an X-Y traversing table to obtain velocity measurements in the required plane.

Seeding particles were generated by atomizing the same fluid employed for oil smoke visualizations further diluted. LDA measurements were acquired at the same time of HWA measurements: in order to get simultaneous (synchronized) LDA and HWA signals, a reference step signal was generated at the beginning and at the end of the acquisition period and it was sent to both LDA and HWA acquisition systems to trigger the measurements, as sketched in figure 3. The lag introduced by the signal generation and by the acquisition systems can be assumed as constant and negligible with respect to the time scales of the physical phenomenon, therefore it does not affect the quality of results in the phase averaging process explained below.

A self-stretched measurement grid of 494 points in X-Y plane is necessary to obtain a complete representation of the velocity vector field around the plates, see figure 2. Even with this large number of LDA measurement points, the X-Y grid has the minimum size necessary to extract the desired information and to correctly identify the vortex structures. The Reynolds number Re=46800 was carefully maintained through a closed-loop control of the wind-tunnel motor. The mean data-rate obtained with LDA measurements is 2000 samples per second and the single point acquisition time is 30 seconds, corresponding to more than 700 mean periods.

To carry out correctly the phase averaging techniques, the HWA reference signal must be acquired without any type of analogue filtering to avoid lags between HWA and LDA measurements.

To reconstruct the main harmonic periods, the HWA signal is digitally filtered without lags, i.e. by a zero-phase digital filter equivalent to a band pass Butterworth filter of order 100; then, the periods are identified by matching the zero-crossings.

3. Data Processing

When a turbulent flow with a periodic mean behavior is considered, the phase averaging technique applied to the LDA measures allows rebuilding the mean velocity field variation over one period. Since the LDA signal is discrete and samples are unevenly distributed in time, a special technique must be used to extract the mean. The reference, nearly periodic signal is divided into short time intervals, called *bins*. Each period is divided in the same number of bins M. If the period has some small fluctuations with time, bins will have slightly different time amplitudes. Let us call N the number of periods. Since some bins do not contain any samples, the number of bins actually depends on the phase angle and will be indicated by $N(\phi)$, where $\phi \in [0°, 360°]$ is the phase angle. In the present case the total number of periods was $N \approx 700$, sufficient to obtain three converged significant figures with M=30 according to Wernert and Favier (1999).

In phase averaging, the first step is to compute the mean velocity value $\mathbf{V}_n$ in every bin n. This is obtained by a transit time weighted average of the LDA signal. Then, the arithmetic mean of such values is taken over all bins with the same phase:

$$\mathbf{V}(\phi) = \frac{1}{N(\phi)} \sum_{n=1}^{N(\phi)} \mathbf{V}_n \,. \tag{1}$$

The x component of the RMS velocity value can be computed by

$$u'(\phi) = \sqrt{\frac{1}{N(\phi)-1} \sum_{n=1}^{N(\phi)} \left\{ \left[\mathbf{V}_n - \mathbf{V}(\phi) \right] \cdot \mathbf{e}_x \right\}^2} \,, \tag{2}$$

where $\mathbf{e}_x$ denotes the x axis unit vector, and similarly for the y component v'.

A key aspect of the phase averaging technique is the correct definition of M: if it is too high, related to the data-rate and to the number of periods, the LDA velocity weighted average value $\mathbf{V}_n$ for a single bin will not be accurate and oscillations in the mean signal will be produced. If it is too low, it will not allow to accurately resolve the mean period, see figure 4.

In the present work, owing to the presence of the two plates, the data-rate is not sufficient to appropriately resolve the mean period by the simple average technique, since the minimum bin duration necessary to obtain a smooth signal would allow for just 10 bins per period, especially for measurement points between the plates. To bypass this problem, a more accurate phase averaging technique is used, the weighted averaging (Sonnenberger et al., 2000). This technique avoids spurious oscillations and allows a better estimate of the RMS value. The signal is obtained by a weighted average on neighboring bins belonging to an overlap interval. For velocity, the weighted mean reads

$$\mathbf{V}_w(\phi) = \frac{\sum_{nb=Ib}^{Fb} I(\phi_{nb})\, \mathbf{V}(\phi_{nb})}{\sum_{nb=Ib}^{Fb} I(\phi_{nb})} \,,$$

where $I(\phi)$ is the total number of valid samples in bins with phase ϕ. $\mathbf{V}_w(\phi)$ does not coincide with the arithmetic mean on the overlap interval due to the transit time weighted average. The RMS velocity weighted average is defined as

$$u'_w(\phi) = \sqrt{\frac{\sum_{nb=Ib}^{Fb} \left[I(\phi_{nb}) - 1 \right] \left[u'(\phi_{nb}) \right]^2}{\sum_{nb=Ib}^{Fb} \left[I(\phi_{nb}) - 1 \right]}} \,.$$

In the present work 30 bins per period have been employed. An overlap interval equal to 24°, corresponding to 2 bins, has been found to be the best compromise between resolution and quality of the signal, as shown in figure 4. In the bin average procedure (2), since one mean velocity value is obtained for each bin, RMS is computed on an actually low-pass filtered velocity signal, the cut frequency being related to the inverse of the bin duration time. Hence, RMS velocity values will be underestimated, since frequencies up to approximately thirty times the main frequency are only retained in the RMS computation. For a thorough analysis of filtering produced damping ratios of the two methods the reader is referred to Sonnenberger et al. (2000).

Once the RMS velocity has been obtained, the (2D) turbulent kinetic energy representing the in plane chaotic contribution can be computed by $k = (u'^2 + v'^2)/2$.

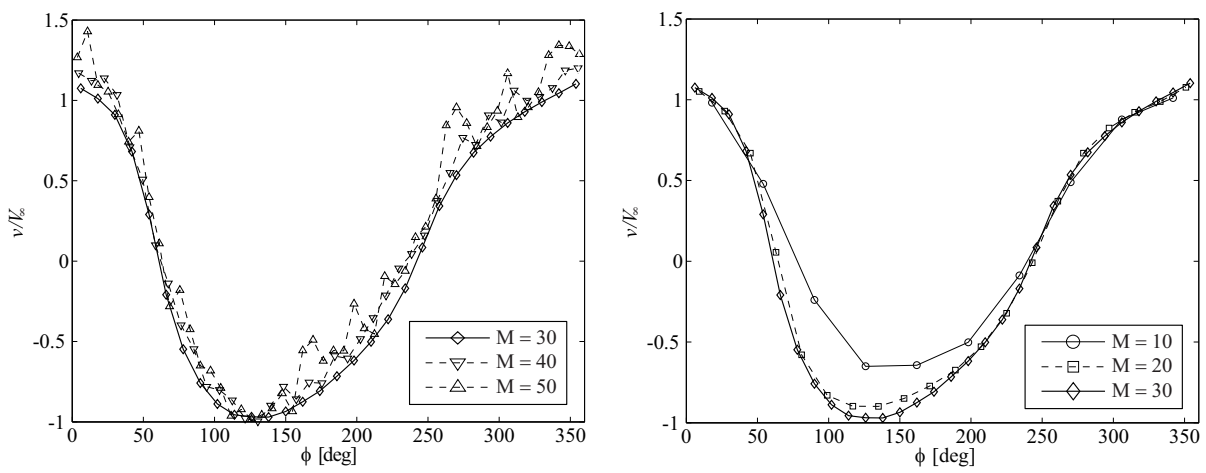

Fig. 4. Phase averaged velocity signal in a measurement point behind the fore plate as a function of the number of bins *M*.

The mean velocity vector fields reported in figure 6 are obtained from the LDA measures using the standard average weighted by the transit time of seeding particles. To better understand the different flow behaviors for small and large gap configurations and to highlight the rotation direction of the vortex structures, the mean vorticity distribution has been computed also. Since the mean flow is 2D, the Z vorticity component of the vorticity vector, computed by second-order finite differences, has been reported.

4. Visualizations

In this section oil smoke visualizations of a full vortex shedding period are reported, see figure 5. Thanks to the short exposure time, visualizations provide many details that help interpreting the flow phenomena. Moreover, the high speed camera employed provided 72 frames per period which allow an accurate tracing of the flow structures. Six frames are reported here for convenience.

The vortex formation and shedding is clearly seen in the visualizations. Visualizations show that the wake vortices form behind the aft plate. For instance in the top half plane in figure 5 (b) and (c), it can be seen that a vortex is detaching. In the next figures, (c) and (d), the shear layer starts rolling behind the aft plate, to form a new vortex in figure 5 (e). The vortex grows, figure 5 (f) , (a) and (b), and the cycle starts again.

A Kelvin-Helmholtz instability can be observed in the shear layers detaching from the fore plate, see in particular the upper shear layer in Fig. 5 (d). For this Reynolds number the shear layer seems to lose stability after a length equal to approximately one third of chord and to produce a rapid transition as witnessed by the rapid diffusion of the smoke afterward.

Figure 5 (d) and (e) show smoke being blown in the gap between the plates from the rearward side, just between the upper shear layer and the upper edge of the fore plate, and forming an eddy structure.

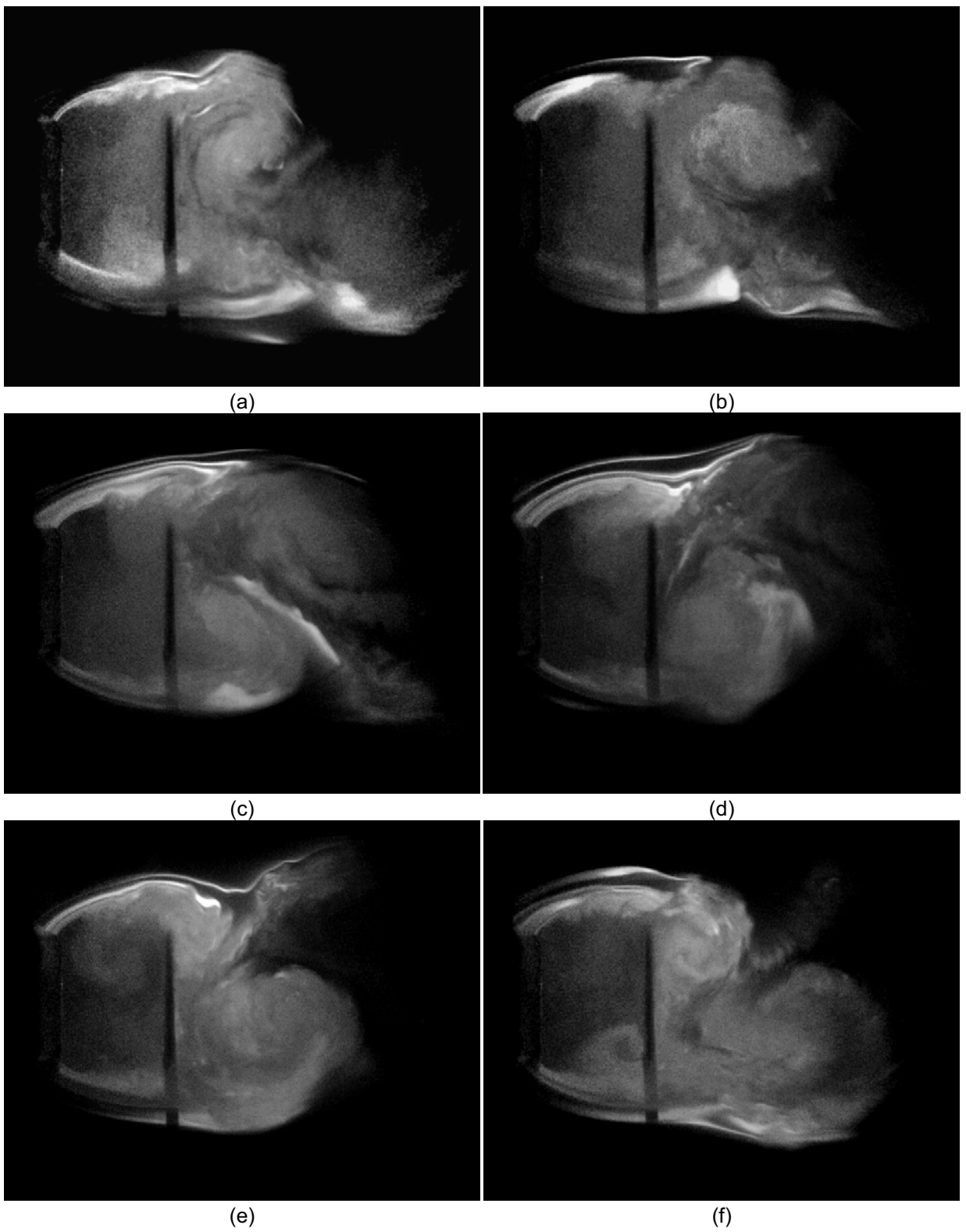

Fig. 5. Visualization of a full period by oil smoke, D/c=0.9, Re=16850.

5. Mean flow and phase averages

In this section the mean and the phase averaged velocity and vorticity fields for the same distance between the plates D/c=0.9 as for the previous visualizations are presented. The mean velocity and vorticity field for D/c=1.2 is also reported here for comparison, while phase averaged velocity fields for this distance are reported in the next section.

The mode I mean flow, shown in figure 6 (a), clearly presents two large recirculating regions behind the second plate. Two recirculating regions are also present between the two plates. Quite surprisingly, however, in these regions the flow rotates the opposite way with respect to the flow in the wake of the aft plate, therefore we will call this behavior "inverse cavity flow". This mode features a wide wake, with large recirculating regions, while mode II, shown in figure 6 (b), displays a narrower wake with quite small recirculating regions, similarly to what found by Lin et al. (2002) for two circular cylinders in tandem configuration.

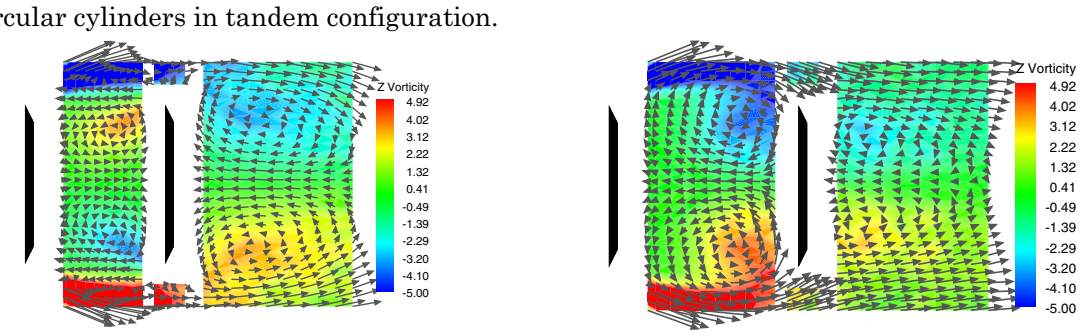

(a) Mode I, D/c=0.9 (b) Mode II, D/c=1.2

Fig. 6. Mean velocity vector fields, Z component of the mean vorticity fields [s^{-1}], Re=46800.

The mean fields do not allow to thoroughly analyze the phenomena involved associated with the time evolution of the flow. This problem can be overcome by analyzing the velocity field during one mean period obtained by the phase averaging technique. Further insight can be obtained from the vorticity component perpendicular to the plate section. Moreover, to better understand the flow, it is useful to integrate the study of the velocity field with the analysis of the turbulent quantities such as the turbulent kinetic energy.

Six phase angles are presented to describe the flow behavior in one period, see figure 7. In the figure, the periodic generation of vortex structures can be clearly seen. The same figure allows also to track the vortex trajectory in the near wake. Alternate vortices form just behind the aft plate without being much affected by its presence. As the vortex forms, a strong counterflow region is observed behind the aft plate. The wake presents also a saddle point which is convected downstream with the vortices, as clearly visible from figure 7 (b) and 7 (c).

A weak recirculating flow which extends beyond the plate edge by almost a quarter of chord is observed between the two plates. In this region velocities are small, and the fluid rotates around two centers that show little displacement during the complete period. As already noted for the mean velocity field, the rotation direction is opposite to that of the vortices shed in the wake. This observation supports the hypothesis that the two plates, for distances lower than their chord, behave basically as a single body because the shear layer detaching near the fore plate does not penetrate the region between the two plates.

As the reverse flow impinges on the back side of the aft plate, its edges act as a trailing edge during all the period. Here two shear layers detach into the cavity region to form the two weak counter-rotating vortices that produce the inverse cavity flow. This phenomenon is well illustrated from figure 7 (b)-(d) for the bottom edge.

The turbulent kinetic energy field with superposed velocity vectors is reported in figure 8 for the same phases. The most evident feature is that the location of maximum turbulent kinetic energy almost coincides with that of maximum vorticity. The same behavior was described by Lyn et al. (1995) for the flow about a square cylinder, and also the turbulent kinetic energy values agree very well. In figure 8 (a) and (d) another strong peak is observed in the k distribution, near to streamline saddles. While other authors have reported peaks in the tangential Reynolds stress near streamline saddles, this peak has not been observed previously, to the authors' knowledge.

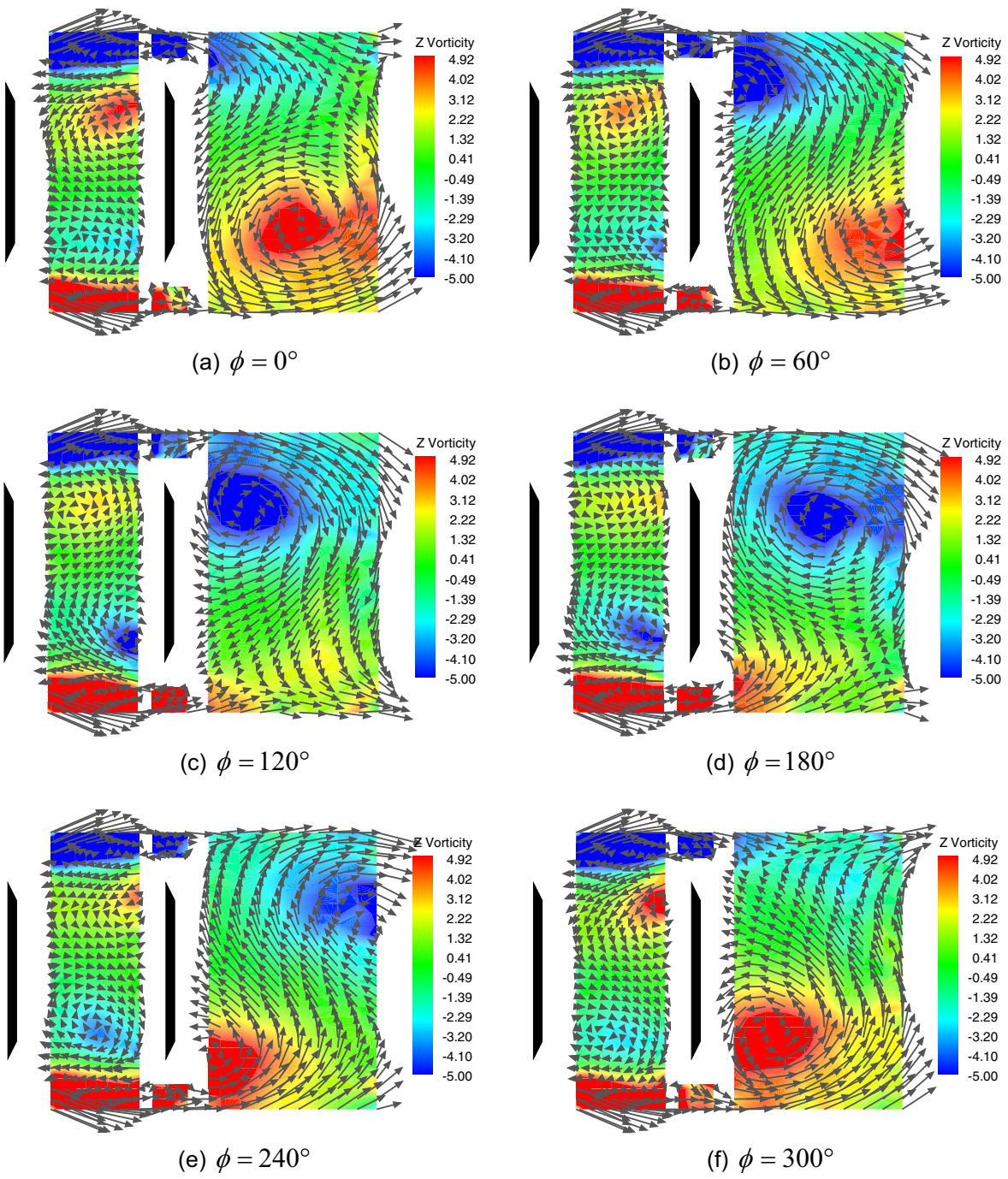

(a) $\phi = 0°$ (b) $\phi = 60°$

(c) $\phi = 120°$ (d) $\phi = 180°$

(e) $\phi = 240°$ (f) $\phi = 300°$

Fig. 7. Instantaneous velocity field, Z vorticity distribution [s^{-1}], Mode I, $D/c = 0.9$, Re=46800.

Between the two plates, where low velocities are measured, low values of *k* are found for the entire period. Two high *k* zones alternately form between the shear layer that detaches from the fore plate and the cavity between the plates. The corresponding kinetic energy is convected in the wake in the center of the shed vortices. In this process *k* starts to be dissipated as its peak level decreases as the vortex is transported downstream.

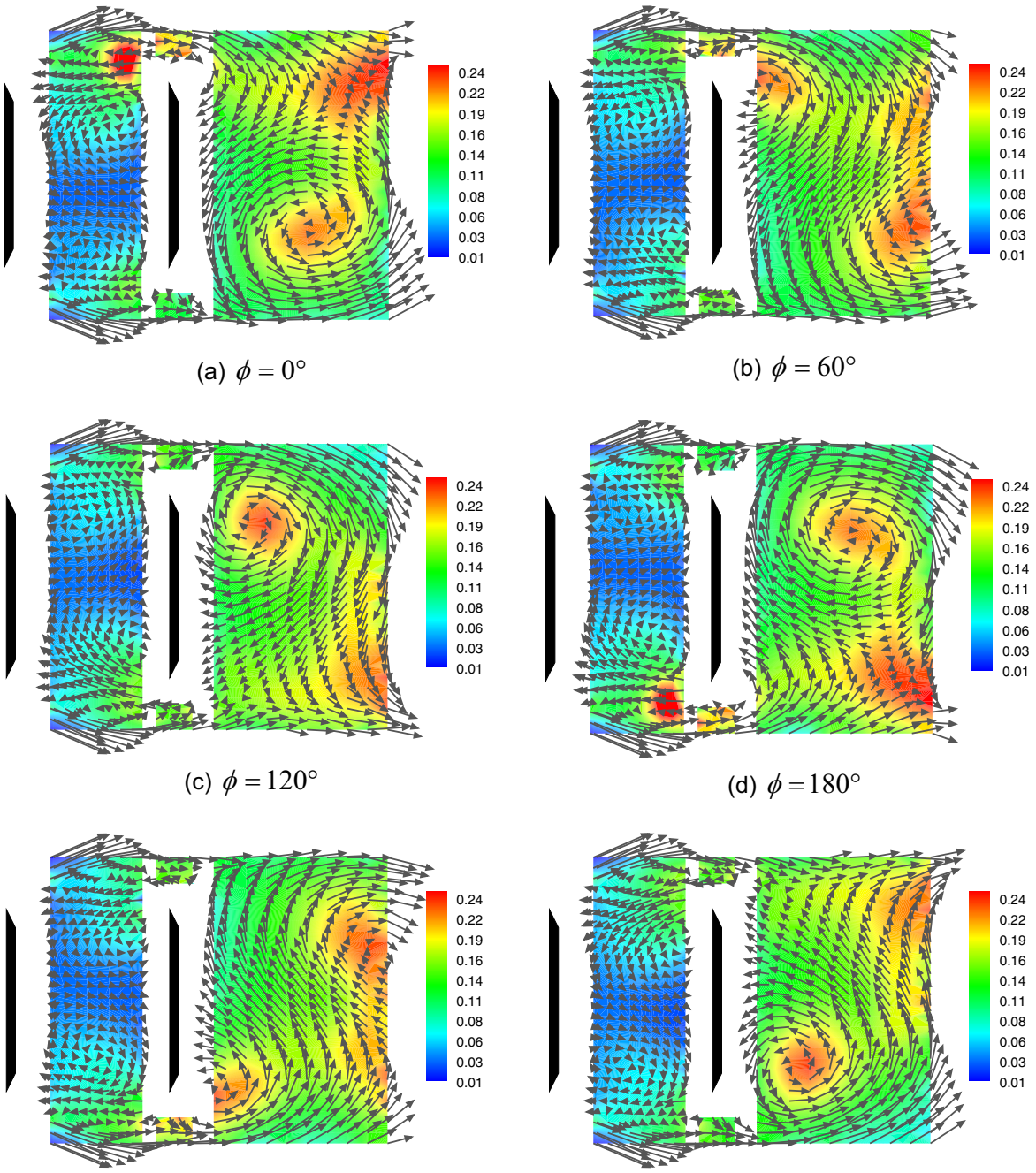

(a) $\phi = 0°$ (b) $\phi = 60°$

(c) $\phi = 120°$ (d) $\phi = 180°$

(e) $\phi = 240°$ (f) $\phi = 300°$

Fig. 8. Turbulence energy field for one period, Re=46800.

6. Comparisons and discussion

It is very interesting to compare visualizations with the more quantitative information obtained from phase averages. The best way to obtain this is to superpose velocity vectors reported in figure 7 to the flow visualizations presented in figure 5. Frames and measurements are equispaced in time.

The first interesting information that is readily obtained is that, despite the difference in Reynolds numbers, the two flows are very similar on a first look. While the fact that the Strouhal number is almost independent on the Reynolds number was known from previous studies (see Auteri

et al., 2008), a direct comparison had not been attempted before.

By investigating pictures in more detail, the first interesting detail that should be noted is that the shear layer behavior is correctly described for all phases and smoke streaks are well aligned with the velocity vectors. Clearly some details are lost in the phase averaged velocity fields since fluctuations occurring at a frequency higher than the shedding frequency are filtered out in the averaging process. The fluctuations, as those generated by the Kelvin-Helmholtz instability, are however witnessed by the turbulent kinetic energy distribution (figure 8).

By exploiting the information coming from visualizations and measurements new insight can be gained on the flow between the plates. In fact, smoke is injected in the gap from the region near the aft plate edges, as clearly visible in the upper portion of figure 9 (c)-(d). Such jets seem to be produced by induction from the near wake vortices, as shown in figure 9 (c). This couple of counter-rotating vortices induces an upstream jet that impinges on the rear side of the aft plate. The jet produces a separation on the aft plate edge and penetrates the region between the plate edge and the fore plate shear layer. Two smoke eddies are formed which rotate in counterclockwise and clockwise direction in the upper and lower part of the gap, see figure 9 (e) and 9 (f), respectively. In summary, the rear plate works in the reverse flow produced by the wake vortices, so that the inverse cavity flow is simply produced by separation of such reverse flow from the aft plate. It is still to be cleared if such phenomenon occurs for every gap width under the critical one or if it is a property of relatively large gaps. This phenomenon is not observed for circular cylinders, probably since the wake of the fore body is narrower leaving no space for an upstream jet to penetrate between the aft cylinder and the fore cylinder shear layer.

It is also interesting to compare Mode I and Mode II flow configurations. By looking at the phase averaged measures reported in figure 10, where Mode II is presented, it is evident that the complex flow field downstream the two plates is caused by the formation and detachment of alternating vortices generated by the roll-up of the shear layers from the fore plate. In fact, in the early stage of vortex formation, fluid and vorticity are transported into the gap between the two plates, see figure 10 (a) and (b). Afterwards, the high vorticity zone in the core of the vortex is pulled away by the opposite shear layer entering the gap, leading the vortex to overtake the aft plate and be released in the wake. It is this mechanism which is probably responsible for the frequency and phase locking of the vortex shedding from the two plates.

Differently from what happens in mode I, vortices must overtake the aft plate to be shed in the wake, figure 10 (c), (d) and (e). This different behavior could be the reason why the Strouhal numbers observed for the two flow configurations are appreciably different. When plates are quite near, the flow behaves as if a single body where present. When the aft plate is moved downstream and the flow behaves as mode II, the shear layer rolls up behind the first plate and strongly interact with the aft plate. The nearer the plates the shorter the time needed by the forming vortex to overlap the aft plate and being shed in the wake. When the distance is further increased, the confinement effect of the aft plate retards vortex detachment, thus decreasing again the shedding frequency.

During the vortex formation phase, the aft plate edge near to the forming vortex acts as a leading edge, while after the vortex has overtaken the plate the same edge acts as a trailing edge, figure 10 (e) and (f). Although there are no measurement points on the plate surface, it is clear that the stagnation points on the two sides of the aft plate move up and down and disappear for the limited time periods during which the plate is nearly parallel to the flow, figure 10 (c). Contrary to what happens for Mode I, in this case a strong jet-like flow induced by the two vortices is directed to the rearward side of the fore plate, where an attachment stagnation point is always present. This phenomenon is analogous to what observed by Lin et al. (2002) for circular cylinders at higher distances.

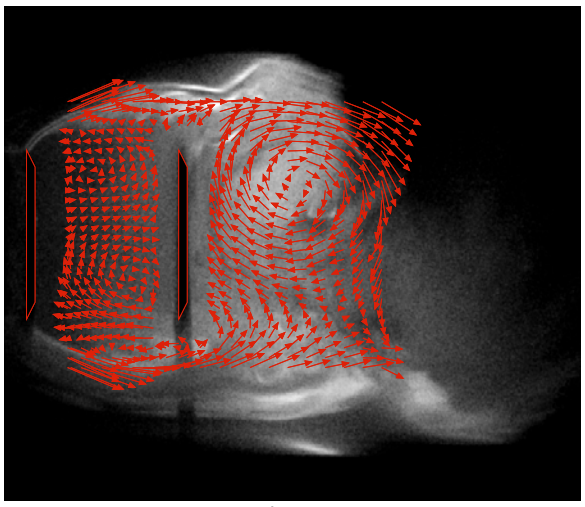

(a) $\phi = 180°$

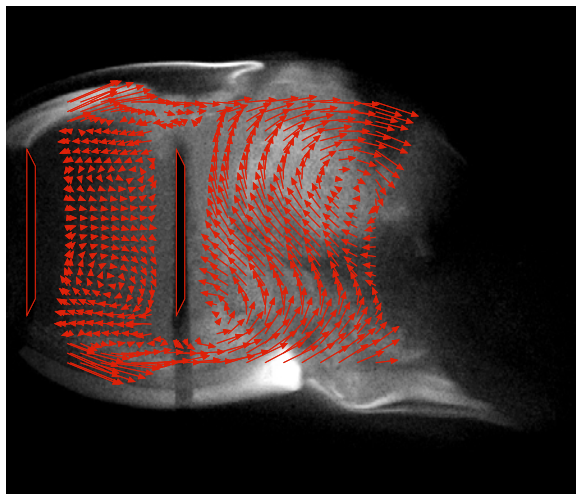

(b) $\phi = 240°$

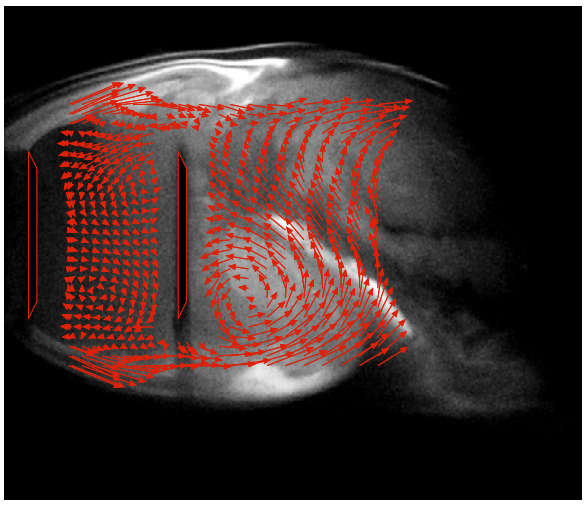

(c) $\phi = 300°$

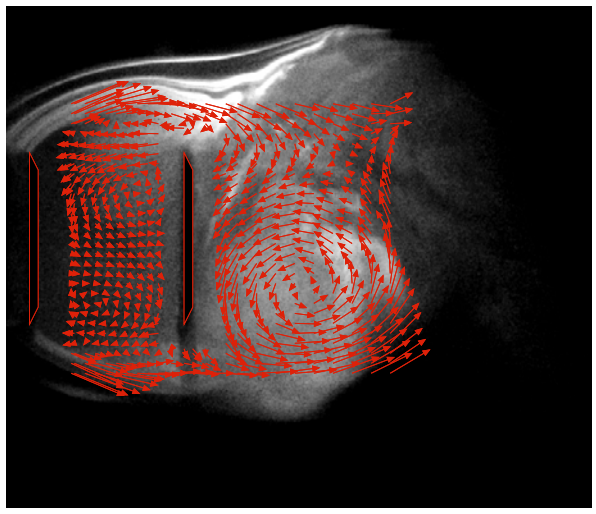

(d) $\phi = 360°$

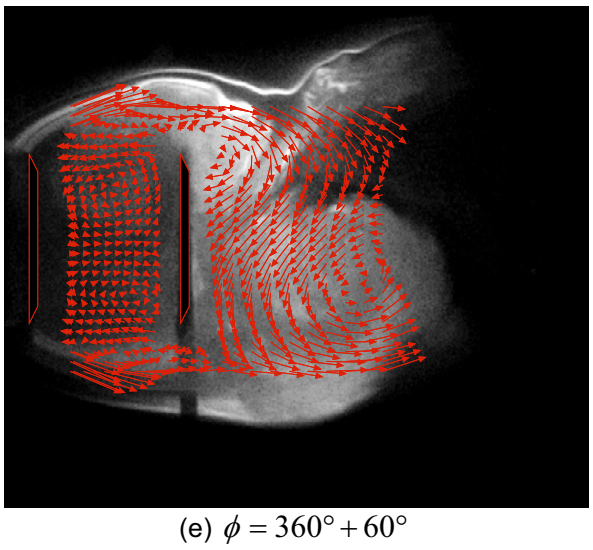

(e) $\phi = 360° + 60°$

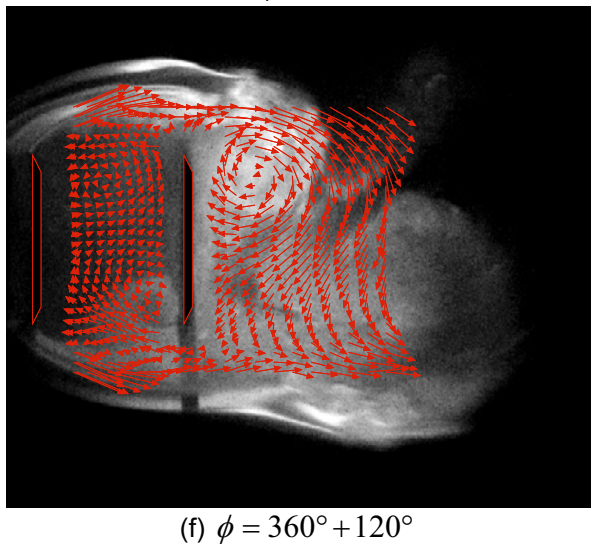

(f) $\phi = 360° + 120°$

Fig. 9. Comparison between visualizations and measurements.

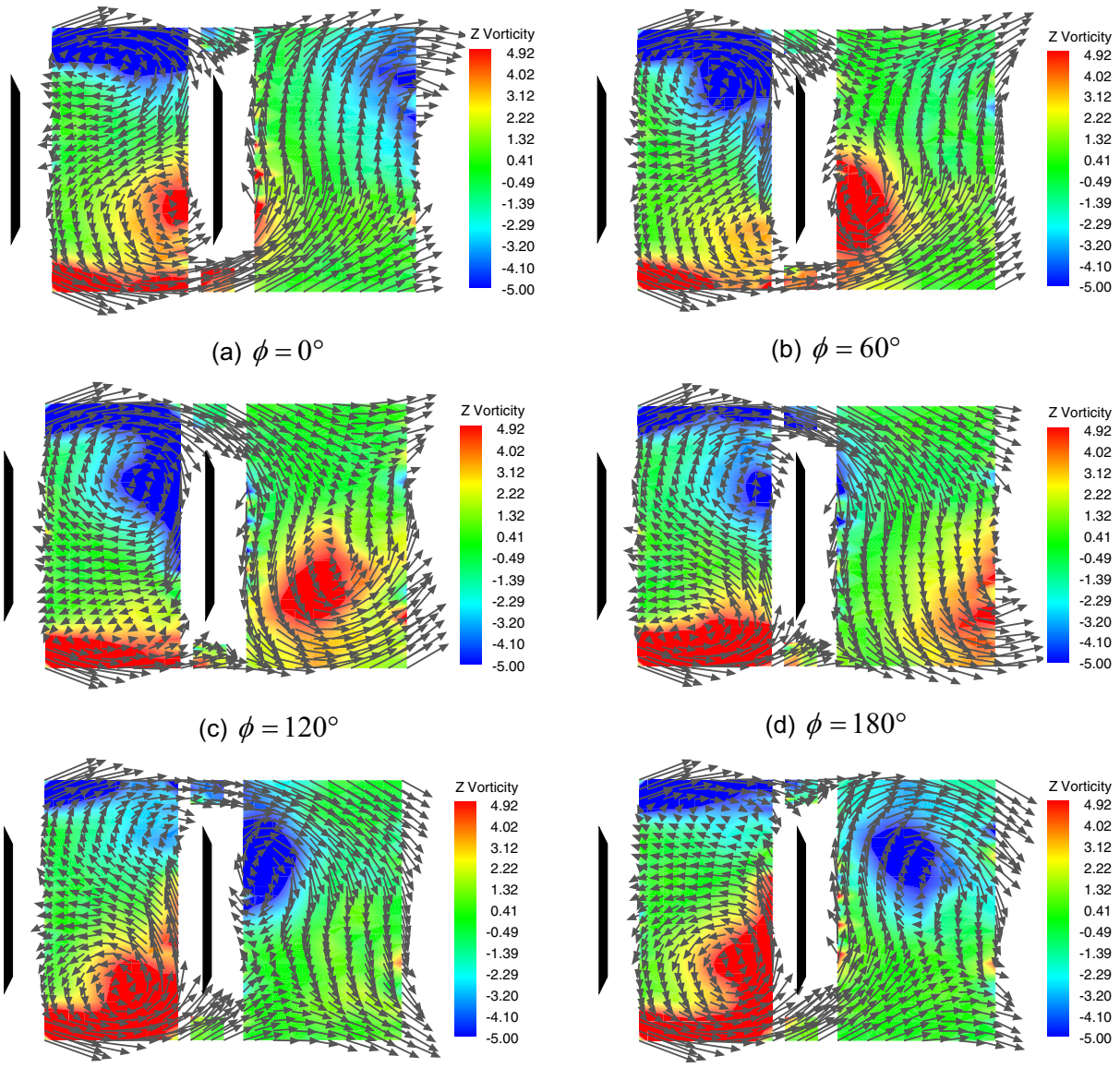

(a) $\phi = 0°$ (b) $\phi = 60°$

(c) $\phi = 120°$ (d) $\phi = 180°$

(e) $\phi = 240°$ (f) $\phi = 300°$

Fig. 10. Instantaneous velocity field, Z vorticity distribution, Mode II, $D/c = 1.2$, Re=46800.

7. Conclusion

In this paper the flow field behind two normal flat plates in tandem configuration has been investigated by two complementary techniques: low exposure time oil smoke visualizations and phase averaged LDA measures. Thanks to frame low exposure times, flow visualizations enable fine details of the flow to be captured. By means of a high speed camera, flow patterns can be traced to obtain a qualitative understanding of the flow behaviour. In the present case, for instance, fine details of the Kelvin-Helmholtz instability of the shear layer detaching from the fore plate can be obtained. In phase averages, while employing a very dense measurement grid to obtain a good spatial resolution, such details are lost both because the space resolution of the measures is not sufficient, but also because the frequency of the Kelvin-Helmholtz instability is not related to the vortex shedding frequency which drives phase averaging. Nevertheless, phase averages provide

necessary quantitative information such as the velocity vector or the vorticity vector, but also other interesting quantities such as turbulence kinetic energy, which are essential to understand the underlying physics and are very useful to interpret visualizations.

There are some important aspects to be taken into account to obtain good results when phase averaging LDA measurements of a flow whose periodicity is not imposed but arises from the instability of the flow itself. First, the physical quantity used for phase referencing must be carefully selected. Second, seeding should be optimized to increase the data rate as much as possible, especially when the flow field geometry makes it difficult for particles to reach some points. Third, for each measurement point a large number of samples should be acquired to obtain accurate averages. In this respect, the weighted phase average technique helps improving results when a suboptimal amount of data is available.

Several pieces of information can be deduced by analyzing and comparing both visualizations and measurements. Owing to the particular shape of the investigated geometry and up to the investigated Reynolds numbers, Reynolds number seems not to affect the flow in the larger scales. For small plate distances, say less than one plate chord, the shear layer detaching from the fore plate rolls up behind the aft plate. This fact has two consequences: the observed Strouhal number does not differ significantly from that of the isolated flat plate; the aft plate is immersed in the wake back flow produced by the fore one and thus producing a low velocity zone in the gap between the plates with two recirculating cells rotating in the opposite direction with respect to the wake vortices.

Overall this flow has several common features with the flow around two in tandem circular cylinders. The unstable character of the shear layers detaching from the fore body is observed. For low distances between the plates, the vortices roll up in the wake of the aft plate. For distances lower than the critical one the flow in the gap region is weak. Despite these similarities, some notable differences with respect to the circular cylinders are: differently from what found by Lin et al. (2002), no asymmetry of the mean flow field has been observed in this case. Moreover, for the tested distance, an inverse rotating flow is present in the gap. Further investigation will be necessary to understand if this phenomenon is restricted to a narrow range of gap spacing or if it characterizes the mode I.

References

Kim, K. C., Lee, M. B., Yoon, S. Y., Boo, J. S. and Chun, H. H., Phase averaged velocity field in the near wake of a square cylinder obtained by a PIV method, Journal of Visualization, 5 (2002), 29-36.

Zdravkovich, M.M., Review of flow interference between two circular cylinders in various arrangements, J Fluids Eng, 99 (1977), 618-633.

Igarashi, T., Characteristics of the flow around two circular cylinders arranged in tandem, 1st. report Bull JSME, 24 (1981), 323-331.

Igarashi, T., Characteristics of the flow around two circular cylinders arranged in tandem, 2nd. report Bull JSME, 27 (1984), 2380-2387.

Lin, J.C., Yang, Y. and Rockwell, D., Flow past two cylinders in tandem: instantaneous and averaged flow structure, J Fluids Struct., 16 (2002), 1059-1071.

Jester, W. and Kallinderis, Y., Numerical study of incompressible flow about fixed cylinder pairs, J Fluids Struct., 17 (2003), 561-577.

Xu, G. and Zhou, Y., Strouhal numbers in the wake of the inline cylinders, Experimental in Fluids, 37 (2004), 248-256.

Takeuchi, T. and Matsumoto, M., Aerodynamic response characteristics of rectangular cylinders in tandem arrangement, J Wind Eng Ind. Aerodyn., 41-44 (1992), 582-600.

Luo, S.C., Li, L.L. and Shah, D.A., Aerodynamic stability of the downstream of the two tandem square-section cylinders, J Wind Eng Ind. Aerodyn., 79 (1999), 79-103.

Havel, B., Hangan, H. and Martinuzzi, R., Buffeting for 2D and 3D sharp-edged bluff bodies, J Wind Eng Ind. Aerodyn., 89 (2001), 1369-1381.

Xu, S.J., Zhou, Y. and Mi, J., Flow visualization behind a streamwise oscillating cylinder and a stationary cylinder in tandem arrangement Journal of Visualization, 7 (2004), 201-208.

Liu, C.H., and Chen, J.M., Observation of hysteresis in flow around two square cylinders in a tandem arrangement, J Wind Eng Ind. Aerodyn., 90 (2002), 1019-1050.

Auteri, F., Belan, M., Gibertini, G. and Grassi, D., Normal flat plates in tandem: an experimental investigation, J Wind Eng Ind. Aerodyn., 96 (2008), 872-879.

Ota, T., Okamoto, Y. and Yoshikawa, H., A correction formula for wall effects on unsteady forces of two-dimensional bluff bodies, J Fluids Eng, 116 (1994), 414-418.

Auteri, F., Belan, M., Cassinelli, C. and Gibertini, G., Two interacting wakes of two flat plates, BBAA VI International Colloquium, 2008.

Domnick, J. and Martinuzzi, R., A cheap and effective alternative for particle seeding fluid in LDA-applications, Experiments in Fluids, 16 (1994), 292-295.

Cantwell B. and Coles D., An experimental study of entrainment and transport in the turbulent near wake of a circular cylinder, J Fluid Mech, 136 (1983), 321-374.

Perry A.E. and Steiner T.R., Large scale vortex structures in turbulent wakes behind bluff bodies. Part 1. Vortex formation processes, J Fluid Mech, 174 (1987), 233-270.
Kiya M. and Matsumura M., Incoherent turbulence structure in the near wake of a normal plate, J Fluid Mech, 190 (1988), 343-356.
Lyn, D.A, Einav, S., Rodi, W. and Park, J.-H., A laser-Doppler velocimetry study of ensemble-averaged characteristics of the turbulent near wake of a square cylinder, J of Fluid Mechanics, 304 (1995), 285-319.
Göttlich, E., Neumayer, F., Woisetschläger, J., Sanz, W. and Heitmeir, F., Investigation of Stator-Rotor Interaction in a Transonic Turbine Stage Using Laser Doppler Velocimetry and Pneumatic Probes, J of Turbomachinery, 126 (2004), 297-305.
Seelhorst, U., Beensten, B.M.J. and Butefish, K.A., Flow field investigation of a rotating helicopter rotor blade by three-component laser Doppler velocimetry, AGARD CP 55 (1994).
Wernert, P. and Favier, D., Considerations about the phase averaging method with application to ELDV and PIV measurements over pitching airfoils, Experiments in Fluids, 27 (1999), 473-483.
Sonnenberger, R., Graichen, K. and Erk, P., Fourier averaging: a phase averaging method for periodic flow, Experiments in Fluids, 28 (2000), 217-224.

Author Profile

Franco Auteri: He received his MSc. degree in Aeronautical Engineering in 1996 from Politecnico di Milano and his Ph.D. in Aerospace Engineering in 2000 from the same university. He has been working in the Aerodynamics Laboratory of the Aerospace Engineering Department, Politecnico di Milano, since 2001. He became assistant professor of fluid dynamics at the Industrial Engineering Faculty of Politecnico di Milano in 2005. His research interests are related to experimental and computational fluid mechanics.

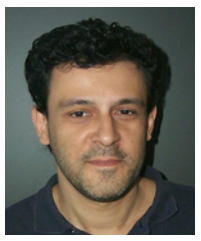

Marco Belan: He received his MSc. in Physics in 1991 from Università di Torino and his Ph.D. in Aerospace Engineering in 1995 from Politecnico di Torino. He has been working in the Aerodynamics Laboratory of the Aerospace Engineering Department, Politecnico di Milano, since 1999. He is now assistant professor of aerodynamics, his main research topics belong to experimental fluid dynamics and applied mathematics.

Carlo Cassinelli: He received his MSc. degree in Aeronautical Engineering in 2008 from Politecnico di Milano. He worked in the second half of 2008 in the Aerodynamic Engineering Research Laboratory of Politecnico di Milano as research associate collaborating to the present work on bluff body aerodynamics. Then, he left Politecnico to join AgustaWestland where he is presently employed.

Giuseppe Gibertini: He received his MSc. degree in Aeronautical Engineering in 1987 from Politecnico di Milano. He received a post-graduate Diploma in Fluid Dynamics in 1988 at Von Karman Institute then he rejoined the Politecnico where he obtained the Ph.D in Aerospace Engineering in 1992 with a thesis on “Separated turbulent flows”. He is now assistant professor at Politecnico di Milano where he is in charge of the Experimental Fluid Dynamic course since 1999. His current main research interests are bluff bodies fluid dynamics and unsteady aeronautical aerodynamics.